Available online at www.sciencedirect.com

jmr&t Journal of Materials Research and Technology

www.jmrt.com.br

Original Article

Nanofiltration membranes prepared from pristine and functionalised multiwall carbon nanotubes/biopolymer composites for water treatment applications

Ahmed A. Alshahrani[a,*], *Ibrahim Hotan Alsohaimi*[b,*], *Saad Alshehri*[c], *Alshaima R. Alawady*[d,e], *M.R. El-Aassar*[b,f], *Long D. Nghiem*[g], *Marc in het Panhuis*[h]

[a] *National Centre for Radioactive Waste Treatment, King Abdulaziz City for Science and Technology, Riyadh 11442, Saudi Arabia*
[b] *Chemistry Department, College of Science, Jouf University, Sakaka 2014, Saudi Arabia*
[c] *National Centre for Radiation Detector Technology, King Abdul Aziz City for Science and Technology, Riyadh 11442, Saudi Arabia*
[d] *Chemistry Department, College of Science, King Saud University, Riyadh 12372, Saudi Arabia*
[e] *Petrochemicals Department, Egyptian Petroleum Research Institute, Cairo 11727, Egypt*
[f] *Polymer Materials Research Department Advanced Technology and New Material Institute, City of Scientific Research and Technological Applications (SRTA City), New Borg El-Arab, Egypt*
[g] *School of Civil and Environmental Engineering, Faculty of Engineering and IT, University of Technology Sydney, Australia*
[h] *Intelligent Polymer Research Institute, ARC Centre of Excellence for Electromaterials Science, AIIM Facility, University of Wollongong, Wollongong, NSW 2527, Australia*

ARTICLE INFO

Article history:
Received 31 March 2020
Accepted 15 June 2020
Available online 24 June 2020

Keywords:
Buckypapers
Nanofiltration membrane
Chitosan
Water desalination

ABSTRACT

A filtration method was used to prepare buckypaper (BP) membranes for water desalination. The samples are made from a biopolymer (chitosan) containing functionalized multiwall carbon nanotubes (MWCNTs) with $-NH_2$ and $-COOH$ moieties. Comprehensive characteristics of all BP membranes were systematically investigated. This included optimisation of sonication time, electrical and mechanical properties (ranging from 7 ± 1 to 69 ± 1 S/cm and tensile strengths between 17 ± 2 and 60 ± 2 MPa, respectively), contact angle ($36 \pm 3^\circ$ to $105^\circ \pm 2^\circ$), morphology, surface area (ranging from 12 ± 2 m^2/g to 112 ± 4 m^2/g), surface charge, water permeability (from 0.5 ± 0.1 to 6.5 ± 0.2 L/m^2 h bar), and salt rejection. The results indicate that the properties of the BP membrane have been significantly affected as the top layer by the type of multi-walled carbon nanotubes. With MWCNTs–COOH / chitosan BP membranes, the highest permeability towards water was achieved while the MWCNTs-NH_2/chitosan membranes provided the best performance in salt rejection by properly balancing amine groups on the top layer, which could be separate monovalent and multivalent cations from salt solutions. Moreover, for monovalent cations (e.g. Na^+) BP

* *Corresponding authors.*
E-mails: ashahrni@kacst.edu.sa (A.A. Alshahrani), ehalshaimi@ju.edu.sa (I.H. Alsohaimi).
https://doi.org/10.1016/j.jmrt.2020.06.055

membranes (MWCNTs/chitosan and MWCNTs-NH_2/chitosan) with sufficiently balanced amine groups on the top layer are shown to be much bigger rejection than for higher-valent cations (e.g. Mg^{2+}).

1. Introduction

Water is the Earth's most fundamental resource for life and is becoming perilously scarce and befouled. Due to the growing population, the need for drinking water over the past few decades is growing rapidly. Large global population is affected by scarcity of fresh water [1]. Water contamination is a global problem caused by municipal, industrial, and agricultural wastewaters. In order to overcome the problem of water scarcity, the need to build effective and sustainable technology has arisen in order to increase water supply beyond traditional means.

These technologies provide high quality water despite the feed is wastewater [2–4], seawater [4–7], or brackish water [3,4,7]. Moreover, membrane technologies require less energy than conventional thermal methods. According to Jay R. Werber et. al. [7], thermal desalination technologies consume five times the energy used in membrane technology. Membrane technology may play a significant role in purifying and desalinating water.

Membrane filtration includes ultrafiltration (UF), nanofiltration (NF), and reverse osmosis (RO) membranes in which pressure is used for separation through a semipermeable membrane. The pressure required in such process consumes up to 65%–85% of total energy required by the whole process. Consequently, energy required for water purification is approximately 25% of total water price [7–9]. Therefore, minimizing energy consumption, while improving membrane efficiency, will lower the cost of clean water production. Nevertheless, achieving water permeability might come on the expenses of the selectivity of removing solutes and pollutants.

An extensive research in this field has been employed to overcome permeability and selectivity conflict (see, for example, [10]). Hybrid membrane is one of the most convenient and efficient approach to overcome the permeability-selectivity tradeoff [6–9]. These membranes are composed of organic components, mainly polymer, and inorganic components, such as zeolite [11,12], graphite oxide [13,14], silica [15,16] and multiwall carbon nanotubes (MWCNTs) [17–21].

In both academia and industry, MWCNTs draw significant attention owing to their prominent mechanical, electrical, and thermal features [22–24]. The substantial mass transport ability of MWCNTs has also been gaining considerable interest [25–27]. In addition to their low biofouling properties, MWCNTs, with core diameters as small as 0.4 nm, have shown substantial separation performance [21,28,29]. Therefore, MWCNTs membranes demonstrate promising potential in the water treatment sector, especially in the desalination process. For example, Ludovic F. Dumée et. at [30]. developed self-supporting BP membrane that exhibited 99% salt rejection and a flux rate of ~12 kg/m^2.h.

On the other hand, dispersants are essential for the preparation of BP membranes. This is due to the tendency of MWCNTs to form agglomerates as a result of van der Waals attraction [21,31]. Moreover, the functionalization process of MWCNTs prevents agglomeration and improves the interfacial adhesion between polymer and the graphitic sidewalls of the nanotubes. The functionalization process can be either covalent or non-covalent [31].

With respect to the non-covalent functionalization process, it can be achieved using surfactant-assisted dispersion and polymer wrapping [31]. Surfactant-assisted dispersion requires, with the assistance of surface-active molecules such as sodium dodecyl-sulfate (SDS) or Triton X-100, the transition of MWCNTs to aqueous phase. The formation of aggregates is efficiently prevented by the physisorption of surfactant on the surface of nanotubes. In addition, the existence of aromatic moieties on the surface of surfactant molecules leads to π–π combination with MWCNTs, resulting in more efficient dispersion [32,33]. Polymers, such as, polystyrene [34] or poly(ether-imide) [35], are applied in polymer wrapping to form MWCNTs suspension. Similar to surfactants, polymer chains containing aromatic rings exhibit van der Waals associations and π–π stacking with MWCNTs, resulting in increased dispersion [36–38]. It was found that the surface morphology of the BP membrane was highly dependent on the dispersants used [39,40].

Biopolymers are polymers that are produced by living organisms. Biopolymer applications rapidly expand due to its biocompatibility and biodegradability that meet the growing need to develop bio-based products. Chitosan is the second most common polymer on earth right after cellulose. Chitosan is a natural polysaccharide derived from the process of chitin deacetylation [21].

The deacetylation degree regulates the chitosan solubility in acidic medium as well as the tendency to form huge structures by hydrogen bonding [41–43]. Chitosan has a wide range of applications, including drug carriers, food packaging films and bone substitutes, due to high biocompatibility, non-toxicity, antifungal and antimicrobial activities [44]. Moreover, chitosan high moisture permeability is an attractive feature for conducting research in the field of water treatment membranes [45,46]. The chemically active amine and hydroxyl groups in chitosan structure can be altered and get involved in hydrogen or coulombic interaction [46]. L. J. Sweetman et.al [47]. have been integrated single-walled carbon nanotubes (SWCNTs) into a chitosan matrix via a dispersion-based freeze dry method. Similarly, aqueous solutions of chitosan have been used as selective dispersants for multi-wall carbon nanotubes (MWCNTs) [48].

This study explores the potential of BP membranes for water desalination using different carbon nanotubes,

which are: MWCNTs, MWCNTs−COOH, and MWCNTs-NH_2. In the fabrication process of all BP membranes, chitosan is used as bio-polymer dispersant. Hydrophilicity, electrical conductivity, adsorption, and morphology of all BP membranes are investigated. Also, under specific experimental conditions, water flux and rejection properties of the membranes are examined. Systematically explores the primary variables that govern the efficiency of these fabricated membranes.

2. Experimental

2.1. Materials

Nanocyl, Belgium has obtained the unfunctionalized (MWCNTs) and functionalized thin multi-walled carbon nanotubes MWCNTs T−COOH and MWCNTs -NH_2). Both samples of MWCNTs have a purity of 95 percent and were used without further purification. Sigma-Aldrich Chemicals, China, purchased NaCl 99%. In Scharlau, Spain, anhydrous magnesium sulphate ($MgSO_4$) was purchased 98%. 99% $MgCl_2$ was bought from Supply, Australia. Ajax Finechem Pty Ltd., Australia, purchased HCl 32%, methanol 99.8% and ethanol 96%. The rectangular filter paper of polyvinylidene fluoride (PVDF) for MWCNTs suspension purchased from Millipore (measuring ca. 142×75 mm^2 with a pore size 0.22 μm). The 5.0 μm pore-sized hydrophobic PTFE membrane filters were imported from Ireland and used as chitosan solution filtration membranes to eliminate any remaining chitosan particles. In this analysis, both solutions and dilutions are prepared using Milli-Q® water.

2.2. Buckypaper membrane fabrication

2.2.1. Preparation of dispersion solutions

Chitosan solution of 0.2% (w/v) concentration was prepared. Typically, 6 g of chitosan of an aqueous solution including 1% (v / v) CH_3COOH is dissolved in 3 L. Dispersion solutions are prepared by combining chitosan with (MWCNTs, MWCNTs −COOH and MWCNTs -NH_2) in aqueous solution. MWCNTs was added to a dispersant solution at 1:1, w/v and was mixed by sonication. Sonication time was varied to optimise MWCNTs dispersion in solution. The sonication conditions were ~16 W power output, and pulses were 0.5 s 'on' and 0.5 off. The sample bottle was put in a water bath during sonication to prevent temperature rises.

2.2.2. Preparation of buckypapers

Chitosan solution (150 mL), containing 150 mg MWCNTs, MWCNTs−COOH or MWCNTs-NH_2, was diluted to 250 mL and then filtered using a 30–40 mbar vacuum pump using PVDF hydrophobic filter paper (142 mm, 0.22 μm pore size). To avoid evaporative loss, the top of the filtration system was shielded with aluminium foil. The large membrane was located at 21 °C for 24 h between absorbent sheets of paper with smooth glass at the upper and bottom. From the filtrating membrane, the dry BP membrane was then removed.

2.3. Characterisation techniques and instrumentation

BP membranes were characterized and investigated using the following instrumentation methods.

2.3.1. UV–vis-NIR spectroscopy

For all suspended solutions, a Cary ® 500 UV–vis-NIR spectrophotometer has been used to obtain absorption spectra (300–1000 nm). As stated in previous research, the dispersion solutions were first diluted with Milli-Q water to ensure that the measured absorption was within the instrument optimal range [21]. The dispersion solution was placed into a quartz cuvette and the sample UV–vis-NIR spectra at room temperature (about 21 °C) were reported.

2.3.2. Electrical conductivity

Using the two-point probe method [26], the resistance of the fabricated membranes was tested at ambient temperature and 45% ratio of humidity (RH). Our previous work explains the detailed procedure [21]. An arbitrary generator (Agilent 33220A) of waveform was used to slowly add a −0.1 to + 0.1 V DC-voltage bridge. A digital multimeter (Agilent 34410A) was utilized to monitor the responses of current (I) and voltage (V). A five stream lengths from 0.5 to 3 cm, measurements were reported. Using the law of Ohm, electrical resistance was determined as a function of changed length.

2.3.3. Contact-angle measurement

For assess the contact angles, the sessile fall approach and a DataPhysics ® SCA20 Goniometer equipped with a digital camera were applied. Using the accompanying DataPhysics program (SCA20.1), the static contact angle of Milli-Q water droplets (2-μL) on the BP membrane surface was estimated. For at least five different locations on each membrane, the average contact angle was evaluated.

2.3.4. Scanning electron microscope

A JEOL JSM-7500FA SEM obtained the surface morphology and cross section of all BP membranes. The membrane samples were dried at 50 °C at 24 h in an oven and then the nonconductive materials were deposited with gold to enhance imaging. The samples were frozen in liquid nitrogen for cross section images, and snapped open to expose the inside.

2.3.5. Mechanical assessment

Tensile analysis was performed via a tensile tester Shimadzu EZ-S. First, a Mitutoyo IP65 Digital Micrometer was applied to determine the thickness of each membrane sample. The experiment was then conducted at 21 °C.

2.3.6. Surface area and pore-size distribution of membranes

Micrometric ASAP-2020 analyser and Quantachrome Instruments were used to obtain Nitrogen adsorption/desorption technique at 77 K for BP membranes. Prior to testing, pieces of BP samples (4 mm^2) were activated at 80 °C for 16 h under vacuum. The BET method was used to determine the sample surface areas [49]. Barret, Joyner and Halenda (BJH) [40] and Horvath-Kawazoe (HK) [39] methods were applied to estimate the small as well as big pores of the samples.

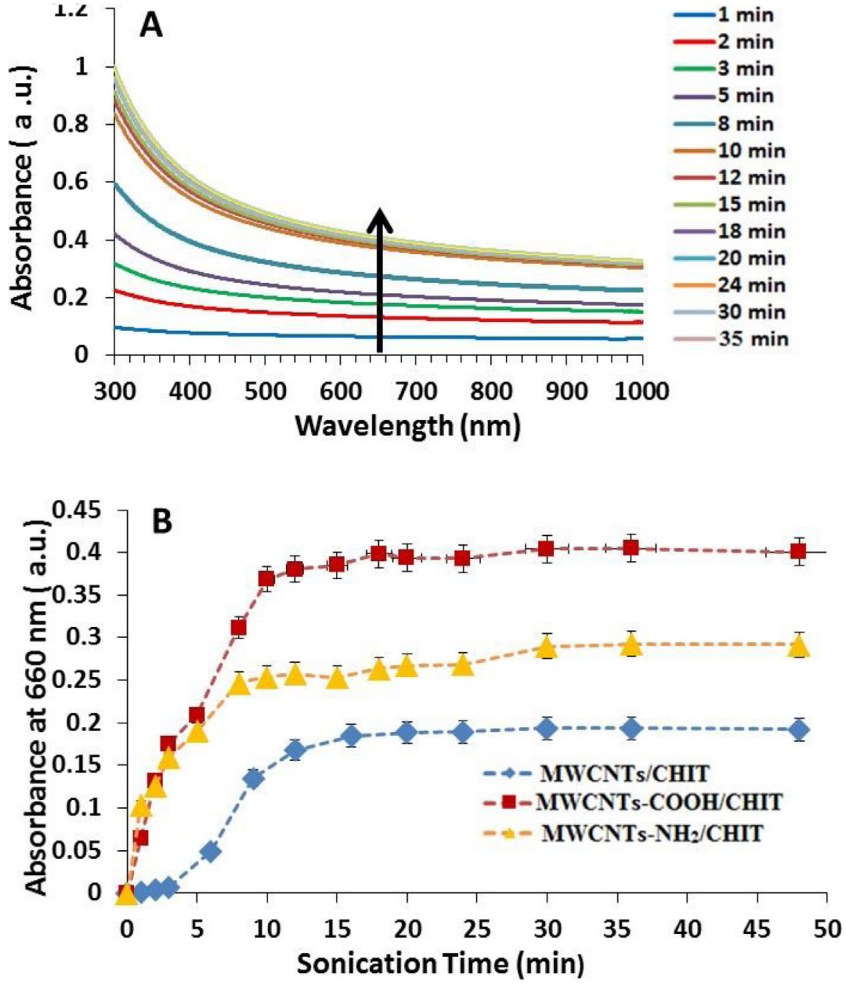

Fig. 1 – A) UV–vis spectra of MWCNTs –COOH/chitosan dispersion as a function of sonication time; B) comparison of the effects of increasing sonication time on the absorbance at 660 nm of MWCNTs /chitosan, MWCNTs–COOH/chitosan and MWCNTs -NH_2/chitosan dispersions.

2.3.7. *Zeta potential*

A SurPASS electrokinetic analyzer (Anton-Paar GmbH, Graz, Austria) has been used to measure the zeta potential (ZP) of all membrane surfaces. The streaming potential measurements of all membranes were performed in 1 mM KCl of background electrolyte solution using the Fairbrother-Mastin method. The pH values for all measurements were systematically estimated by titration using HCl and KOH solutions.

2.3.8. *Permeability and salt-rejection behaviours*

Research lab-scale crossflow NF/RO [21] was extended to evaluate water permeability as well as salt rejection for BP membranes of area 40 cm^2. All measurements were applied using Milli-Q® water. First, all membranes were compressed for almost 1 h at 22 bar pressure. After a steady baseline flux was attained, the water permeability of the membranes was inspected at different pressures. Individual salt solutions 2 g/L (NaCl and $MgSO_4$) were examined to determine salt rejection. A cross flow of 34.7 cm/s with flow 100 L/h was set at 20 °C. Using the Thermo ScientificTM conductivity meter, Orion 4-StarTM, Singapore, salt concentrations in feed and permeate water are calculated. The apparent solute rejection, R (%), for BP membranes were evaluated based on the following equation [21]:

$$R\,\% = \left(1 - \frac{C_p}{C_f}\right) 100\% \quad (1)$$

where C_p and C_f are the permeate and feed solutions concentrations.

3. Results and discussion

3.1. *Optimisation of sonication time*

The sonication of MWCNTs, MWCNTs–COOH and MWCNTs-NH_2 in chitosan was investigated. UV–vis-NIR spectrum (300–1000 nm) of the three dispersions was studied (Fig. 1A). The UV absorbance of each of the three dispersions at 660 nm was plotted against sonication time (Fig. 1B). The wavelength of 660 nm was selected to resist absorbance due to chitosan and Milli-Q water. In agreement with previous researches

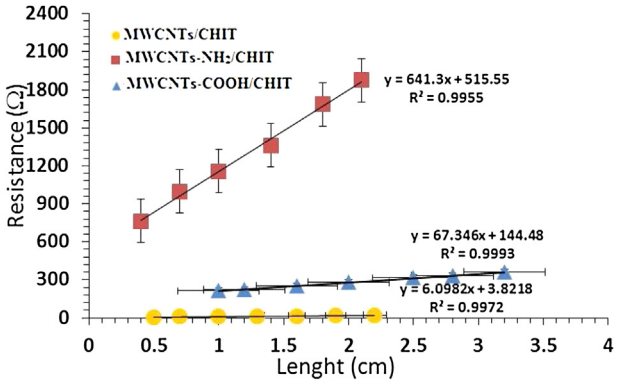

Fig. 2 – Effect of changing the length on the resistance of BP membranes, produced from different dispersions containing 0.2% (w/v) chitosan (CHIT) combined with 0.1% (w/w) MWCNTs, MWCNTs–COOH and MWCNTs-NH_2.

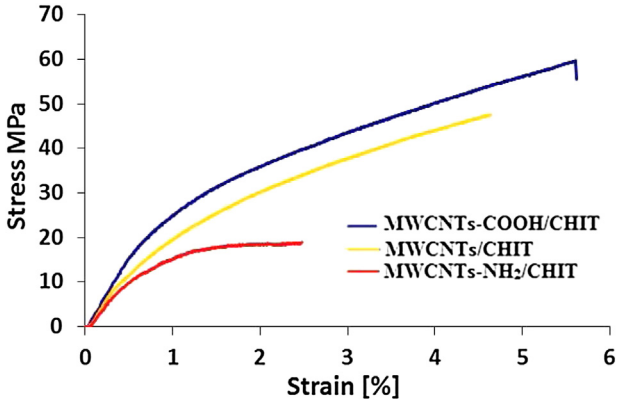

Fig. 3 – Study of the effect of MWCNTs surface modifications and combining chitosan 0.2% (w/v) on the mechanical properties of BP membranes.

[21,26,50], absorbance at (660 nm) was significantly increased by increasing sonication time. The results obtained from the UV–vis-NIR spectra reveal that 12-min sonication were sufficient for the three dispersion solutions (i.e. MWCNTs, MWCNTs–COOH and MWCNTs-NH_2) to be well-dispersed in chitosan solution. No significant changes in the absorption of the three dispersions at 660 nm occurred after 12 min. In addition, 12 min of sonification were sufficient for the three dispersion (MWCNTs, MWCNTs–COOH and MWNT-NH_2). However, from Fig. 1B, a 20 min has chosen for dispersion of MWCNTs and the modified MWCNTs through the solution. Previous studies suggested that CNT would not be dispersed for a long time because the long exposure of ultrasonic energy that is likely to increase defects and reduce the porosity of the buckypaper membranes. This may lead to low mechanical and electronic properties and reduce the efficiency of nanotube carbon membranes to water permeability [51,52]

3.2. *Conductivity of BP membranes*

Electrical properties of BP membranes have substantial impact on their separation performance [53]. The I–V characteristics of all fabricated membranes have therefore been calculated under ambient conditions using the two-point probe approach. The linear relationships shown in Fig. 2 were obtained by Eq. 1, and the conductivity values for the three BP samples are presented in Table 1.

$$R_T = \frac{1}{\sigma A} l + R_c \qquad (2)$$

Where R_T is the overall resistance, A is the cross-section area, σ is the bulk membrane conductivity, *l* is strip length, and R_c is the contact resistance. These results reveal that the conductivity of MWCNTs/chitosan is 69 ± 1, which is much higher than that of the two BP membranes with MWCNTs–COOH/chitosan and MWCNTs-NH_2/chitosan. These significant changes in conductivity can be attributed to the functionalisation process (i.e. attaching –COOH and –NH_2 groups to the surface of MWCNTs s). Hence, carbon atoms hybridization of MWCNTs walls changed from sp^2 to sp^3 [54]. As a Consequence, the electrons cannot easily move on the surface of the membranes owing to the combination between the carboxyl –COOH as well as –NH_2 moieties on the MWCNTs surfaces with a huge number of chemically reactive moieties (-NH_2 and –OH) on the backbone of chitosan. Additionally, the conductivity values correlate well with the results reported for the MWCNTs /chitosan BP membrane prepared using MWCNTs and chitosan [21] as revealed in Table 1.

3.3. *Mechanical properties*

Mechanical strength is of great significance for the fabricated membranes used in separation applications. Membranes designed for water filtration must endure substantial pressure for extended periods. The mechanical properties were therefore examined for the fabricated membranes. Tensile features values (i.e. tensile strength, elongation, toughness and Young's modulus) are illustrated in Fig. 3 and outlined in Table 1. With the exception of MWCNTs-NH_2/chitosan membrane, the values of tensile strength, Young's modulus, elongation and hardness for all membranes fall within a close range. The MWCNTs-NH_2/chitosan BP membrane gave an elongation value of 3.5 ± 0.9%, which was lower than those of the MWCNTs–COOH/chitosan (5.7 ± 0.1%) and MWCNTs/chitosan (4.7 ± 0.7%) membranes. The toughness value for MWCNTs -NH_2/chitosan was significantly low compared to the other BP membranes. In addition, the tensile strengths of both MWCNTs–COOH/chitosan and MWCNTs/chitosan membranes were approximately 3 times higher than that of the MWCNTs-NH_2/chitosan BP membrane. This suggests that there are poor mechanical properties of the membrane (MWCNTs-NH_2/chitosan) relative to the membranes (MWCNTs / chitosan and MWCNTs–COOH / chitosan). On the hand, the tensile strength and elongation of the MWCNTs–COOH/chitosan BP were both slightly higher than the values obtained for the MWCNTs/chitosan BP membrane. This may attribute to strong interactions between the amine group in chitosan chain and the carboxylic group on MWCNTs–COOH. Consequently, MWCNTs carboxylation has

Table 1 – Conductivities, contact angles and mechanical properties of BPs prepared using different types of MWCNTs /chitosan; the errors are represented with standard deviations; values for all BP membranes represent an average of the conductivities of two BPs.

BP membrane	Contact angle (°)	Conductivity (S/cm)	Elongation (%)	Tensile strength (MPa)	Young modulus (GPa)	Toughness (J/g)
MWCNTs/chitosan	105 ± 2	69 ± 1	4.7 ± 0.5	57 ± 3	2.8 ± 0.1	2.1 ± 0.2
MWCNTs-COOH/ chitosan	36 ± 3	7 ± 1	5.7 ± 0.1	60 ± 2	3.3 ± 0.1	2.2 ± 0.3
MWCNTs-NH_2/ chitosan	92 ± 4	1.0 ± 0.3	3.5 ± 0.9	17 ± 2	2.2 ± 0.06	0.5 ± 0.1

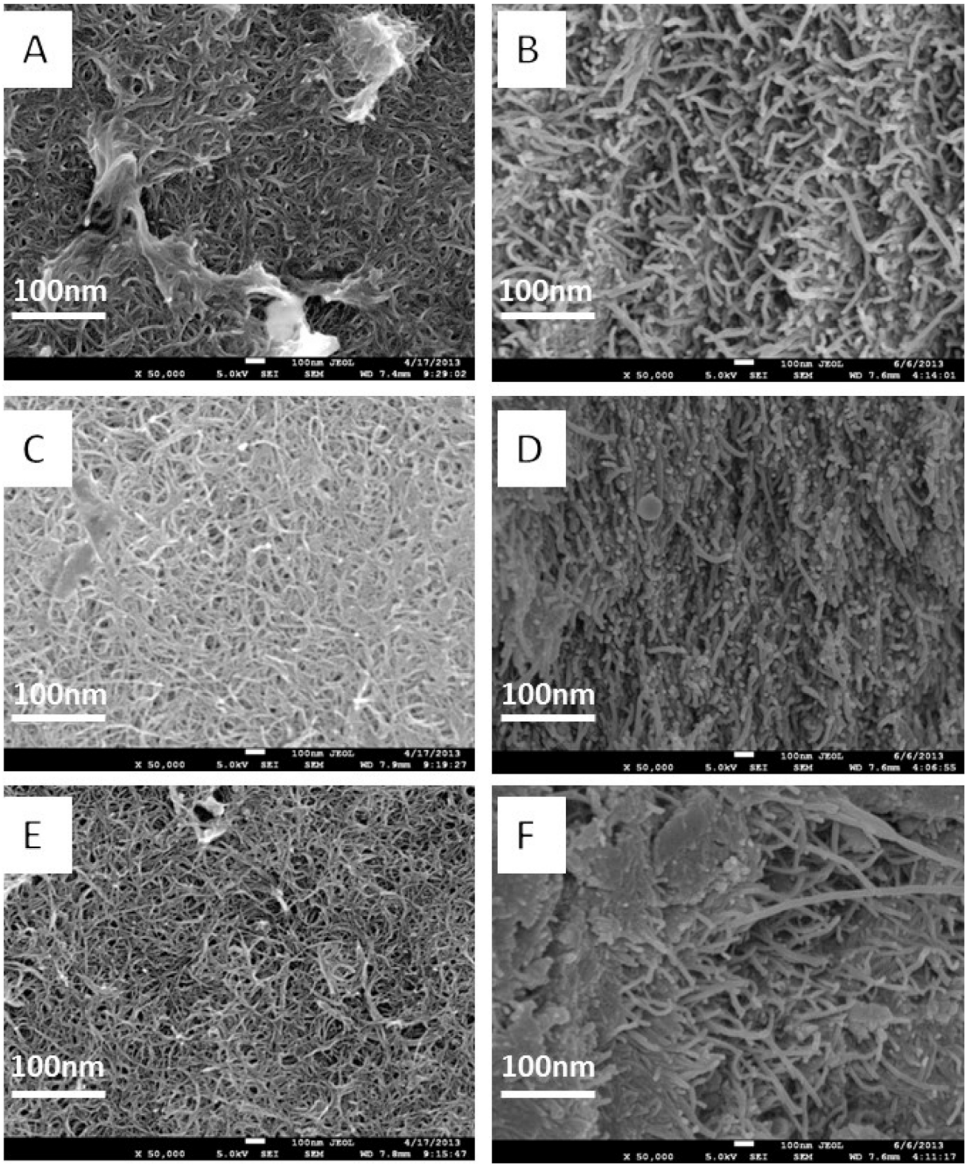

Fig. 4 – SEM images of the surfaces (A, C and E) and cross-sections (B, D and F) of BP membranes formed from (A and B) MWCNTs/chitosan, (C and D) MWCNTs−COOH/chitosan and (E and F) MWCNTs-NH_2/chitosan.

contributed to changes in the mechanical properties of BP membranes. Further, the observation correlates well with the results of the mechanical properties reported here for the MWCNTs/chitosan BP membrane were approximately similar to the mechanical features of BPs fabricated by the vacuum-filtration approach using chitosan and MWCNTs as dispersion [21] as summarised in Table 1.

3.4. *Morphology of BP membranes*

The morphologies of the surface and cross-sections of the fabricated membranes were investigated using SEM technique (Fig. 4) to study the dispersion of MWCNTs, MWCNTs−COOH and MWCNTs-NH_2 in chitosan. SEM images in Fig. 4A, C and E show that the three BP membranes were well dispersed

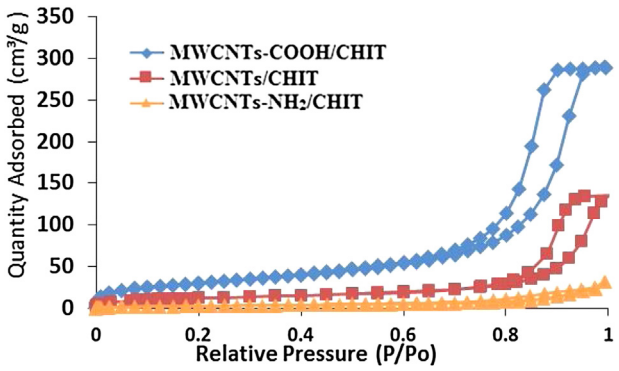

Fig. 5 – Nitrogen adsorption/desorption isotherms for different BP membranes.

in the aqueous solution containing 0.2% w/v of chitosan. Moreover, the dark region on the surface of the BP membranes shows that all membranes possessed a large number of irregularly sized pores aggregated. However, the pores of the MWCNTs−COOH/chitosan BP membrane was slightly larger than those present in the MWCNTs /chitosan and the MWCNTs -NH_2/chitosan membranes. Generally, two BP membranes (MWCNTs/chitosan and MWCNTs -NH_2/chitosan) had very few surface pores. Further, the cross-sections of SEM image (Fig. 4F) showed that NH_2/chitosan BP membrane has fewer aggregates of MWCNTs unlike the other two BP membranes MWCNTs/chitosan and MWCNTs−COOH/chitosan (Fig. 4B, and D). Whitten et al. [55] reported that chitosan MWCNTs can result in larger nanotubes agglomerates to their larger molecular weights than that due to low-molecular-weight surfactants.

3.5. *Assessment of surface characteristics*

The results of N_2 physisorption measurements and BET calculations revealed that the three BP membranes had a popular type IV isotherm with hysteresis loop at relative high pressures (Fig. 5). This hysteresis occurs due to alteration between the adsorbent removal and filling that takes place during a capillary condensation mechanism [53]. The large peaks (blue lines) in Fig. 6 for each BP membrane from 0.5 to 2 nm provide information about the intrabundle pores, whereas the small peaks (dotted lines) from 2 to 10 nm relate to the interbundle pores.

The specific surface area, pore width, pore volume and average bundle diameter for each of the three BP membranes are summarised in Table 2. The MWCNTs -bundle diameter was calculated as described by C J. Frizzell et al. [56]. Overall, the diameters of the nanotube bundles exhibited an inverse of the values of the surface areas of BP membranes. In contrast MWCNTs-NH_2/chitosan, having the lowest surface area (12 ± 2 m^2/g), showed the lowest nanotube-bundle diameters (22 ± 12 nm). While the MWCNTs−COOH/chitosan possessed the largest surface area (112 ± 4 m^2/g) and it demonstrated the slightly large nanotube-bundle diameters (24 ± 3 nm). This is probably owing to the existence of the −COOH moieties, which improve interaction with chitosan while amine groups decrease it. Since better dispersion of MWCNTs within the chitosan solution cause decrease in tangling, folding of the MWCNTs and improvement of their accessibility for nitrogen adsorption [57]. Thus, these results have a substantial effect on the permeability behaviour of water for these BP membranes.

Table 2 illustrates that the three BPs are different in the distributions of their interbundle and intertube pore volumes. For example, the interbundle pore volume of $90 \pm 4\%$ appears to make a larger contribution to porosity in the MWCNTs−COOH/chitosan BP membrane. This value is very near those of MWCNTs/chitosan and MWCNTs-NH_2/chitosan ($82 \pm 2\%$ and $85 \pm 2\%$ respectively). Consequently, the intrabundle pore volume of the MWCNTs -chitosan ($18 \pm 2\%$) was higher than the values obtained for the MWCNTs−COOH/chitosan ($10 \pm 1\%$) and MWCNTs-NH_2/chitosan ($15 \pm 1\%$) BP membranes. The results (surface area, pore diameter, nanotube-bundle diameters and pore-size distribution volume) indicate that functionalization of the MWCNTs surface has a significant effect on the pore-size distribution of BP membranes.

3.6. *Zeta potential*

Surface charge of membranes is a crucial factor for salt rejection. The ZP of the three BP membranes' surfaces were determined and drawn against the pH feed solution (Fig. 7). The ZP measurements for three prepared membranes showed different trends (see Fig. 7). ZP results for MWCNTs-NH_2/chitosan membrane exhibited positive values up to pH 8.4 owing to the protonation of the amine moieties (–NH_2 to –NH_3^+). As the pH increase, ZP started to have negative values. In contrast, MWCNTs−COOH/chitosan membrane displayed negative values of ZP at low pH (e.g. deprotonated −COOH → −COO–) and as the pH rises, the ZP of the membrane starts to give positive values (e.g. protonated –NH_2 → –NH_3^+). This is in agreement with the structure of the membrane. However, MWCNTs/chitosan has almost a neutral surface which is concided with the fact that MWCNTs have no ionisable moieties [58,59]. Previous studies have shown that a more negative membrane is more salt rejected owing to a coulombic interaction between the negatively charged membrane surface and charged solutes [60,61]. The positive values of ZP at pH range of 4–8 suggest that the adsorption of NaCl can be increased by decreasing the pH.

3.7. *Water permeability*

The water permeability of the three BP membranes fabricated was measured via the crossflow NF/RO approach, in which the permeate flux was plotted against the pressure applied (Fig. 8). The permeability findings were estimated on the basis of the slope of the liner correlation between the applied pressure and flux.

The Water permeability of the fabricated BP membranes increased in conjunction with increasing applied pressure. Water permeability of the three BP membranes were in the order MWCNTs−COOH/chitosan > MWCNTs/chitosan > MWCNTs -NH_2/chitosan (Table 2). The average permeability rate of MWCNTs−COOH/chitosan BP membrane was 6.5 ± 0.2 L/m^2 h bar, 16 times greater than that of MWCNTs-NH_2/chitosan

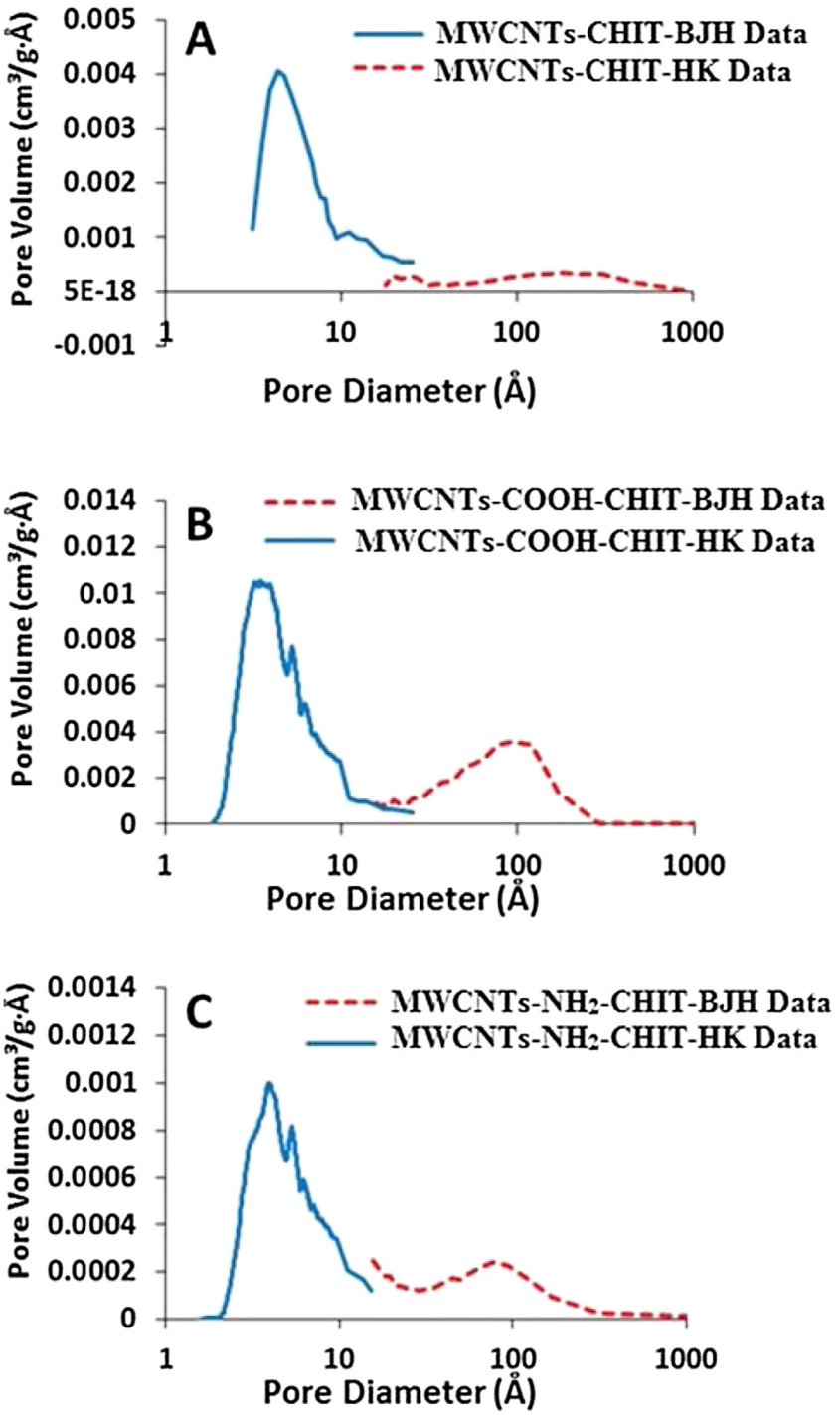

Fig. 6 – Total pore volume as a function of pore diameter for different BP membranes: HK (blue line peak) and BJH methods (orange dotted peak) data obtained from nitrogen adsorption/desorption isotherms for the following: a) MWCNTs/chitosan; b) MWCNTs−COOH/chitosan; and c) MWCNTs-NH_2/chitosan.

(0.4 ± 0.1 L/m^2 h bar) and about 4.5 times higher than that of MWCNTs/chitosan (1.5 ± 0.1 L/m^2 h bar). This due to the presence of a polar group (−COOH) which improved surface hydrophilicity. This complies with contact angle (Table 1) and surface area values (Table 2). On the other hand, MWCNTs-NH_2/chitosan membrane exhibited the lower water permeability than the other two membranes which is consonant with its low hydrophilicity and specific surface area values (Tables 1 and 2).

3.8. *Salt-rejection capability*

A crossflow RO/NF system was used to determine salt-rejection capability of all fabricated membranes. Two inor-

Table 2 – Surface area (A_{BET}), average pore-size diameter (d_{BET}), average bundle diameter (D_{bun}), interbundle pores, intrabundle pores and water permeability of BP membranes prepared by a filtration method.

BP membrane	Surface area (m^2/g)	Average pore size (nm)	Average bundle diameter (nm)	Interbundle pore volume (%)	Intrabundle pore volume (%)	Water permeability (L/h. m^2.bar)
MWCNTs/chitosan	45 ± 2	21 ± 2	59 ± 5	82 ± 2	18 ± 2	1.5 ± 0.1
MWCNTs-COOH/chitosan	112 ± 4	10 ± 1	24 ± 3	90 ± 4	10 ± 1	6.5 ± 0.2
MWCNTs-NH_2/chitosan	12 ± 2	10 ± 1	22 ± 12	85 ± 2	15 ± 1	0.5 ± 0.1

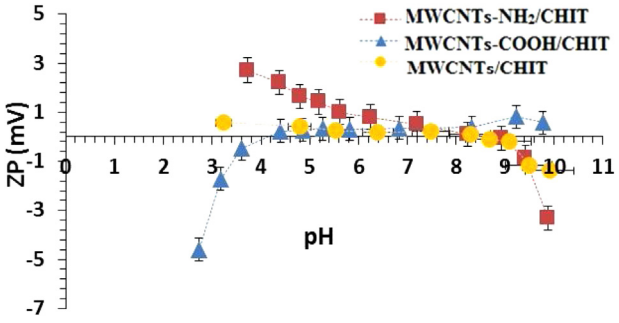

Fig. 7 – Zeta potential ZPs of the membranes as a function of pH.

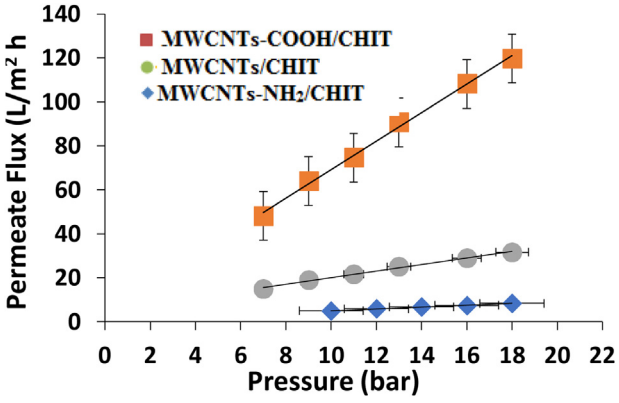

Fig. 8 – Effect of different applied pressures on permeation flux of the three BP membranes.

ganic electrolytic solutions NaCl, and $MgSO_4$ of concentrations 2 g/L were investigated as a single salt aqueous solution. Each salt rejection was plotted against the pressure applied (Fig. 9 A and B). For all BP membranes, salt rejection increases with rising applied pressure which indicates that gradually increasing the applied pressure (7–18 bar) progressively increases salt-rejection levels owing to the 'dilution effect' [62–64].

The salt-rejection of all fabricated BP membranes increased in conjunction with increasing applied pressure. The salt-rejection of the three BP membranes were in the order MWCNTs-NH_2/chitosan > MWCNTs/chitosan > MWCNTs−COOH/chitosan (Fig. 9 A–B). The MWCNTs-NH_2/chitosan BP membrane exhibited greater salt rejection than that salt rejection of MWCNTs/chitosan and MWCNTs−COOH/chitosan. This may be due to more amine groups (NH_2) on the MWCNTs-NH_2/chitosan BP membrane structure, which may increase the membrane's surface charge densities. On the other hand, Fig. 9 A—B show that the MWCNTs−COOH/chitosan BP can be as an ultrafiltration (UF) membrane, as it has lower salt rejection for both of the single salts (NaCl and $MgSO_4$). It appears that the base composite BP membrane (MWCNTs−COOH/chitosan) situ amine cross-linked with MWCNTs−COOH affects the characteristics of the top layer. The significance of the effect on solute retention based on the pore distribution and the membrane size. Huiqing with his group reported that molecules of water and egg albumin can simply pass through a multi-walled carbon nanotubes/polymer composite due to the gaps are large enough. Consequently, the water flux increases and the rejection decreases by a multi-walled carbon nanotubes/polymer composite membranes [65]. Adsorption and exclusion by size contribute to the retention of the solute according to the pore size [66]. Further, MWCNTs−COOH/chitosan BP membrane exhibited the lowest salt rejection consonant with its hydrophilicity (36° ± 3°), great specific surface area value (112 ± 4 m^2/g) and high water permeability (6.5 ± 0.2) as shown in Tables 1 and 2.

Furthermore, the observed single salt-rejection order as seen in Fig. 9 A and B, is R($MgSO_4$) < R(NaCl), illustrating that the salt-rejection pattern of MWCNTs /chitosan membranes is positively charged in accordance with the Donnan principle. Additionally, the lower rejection level of $MgSO_4$ can be justified by the decrease in the effective charge on surface of the membrane, due to the combining of anions of SO_4^{2-} and Mg^{2+}, which leads to decreased rejection performance [61,67]. However, these results contradict some previous research indicating that R(NaCl) < R($MgSO_4$) [37,39], which can be ascribed to the Donnan feature of salt rejection on negatively charged NF membranes. The degree of rejection also depends on the valence of the electrolytes, and several studies have found that the rate of rejection of salts with the same cation (Na^+) is greater for divalent anions SO_4^{-2} than monovalent ions (Cl-), and that with monovalent counter-ions (Na^+) electrolytes have a higher rate of rejection than divalent counter-ions (Mg^{2+}) [40].

The surface charge depends on the ionisation level and, thus, the pH of the aqueous solution. The membrane with amine groups could have a positive charge when pH is low (e.g. protonated ($-NH_2 \rightarrow -NH_3^+$), and the surface of the membrane with carboxyl groups could have a negative charge when pH ranges from moderate to high. The fabricated buckypaper membranes (MWCNTs/chitosan, MWCNTs−COOH/chitosan and MWCNTs-NH_2/chitosan) were used at various pH values (ranging 10–3) with constant temperature of 20 ± 2 °C to investigate NaCl (concentration 2 g/l) rejection. The pressure was tuned to acquire the same permeate flux for three BP membranes and the results are illustrated in Fig. 10. The

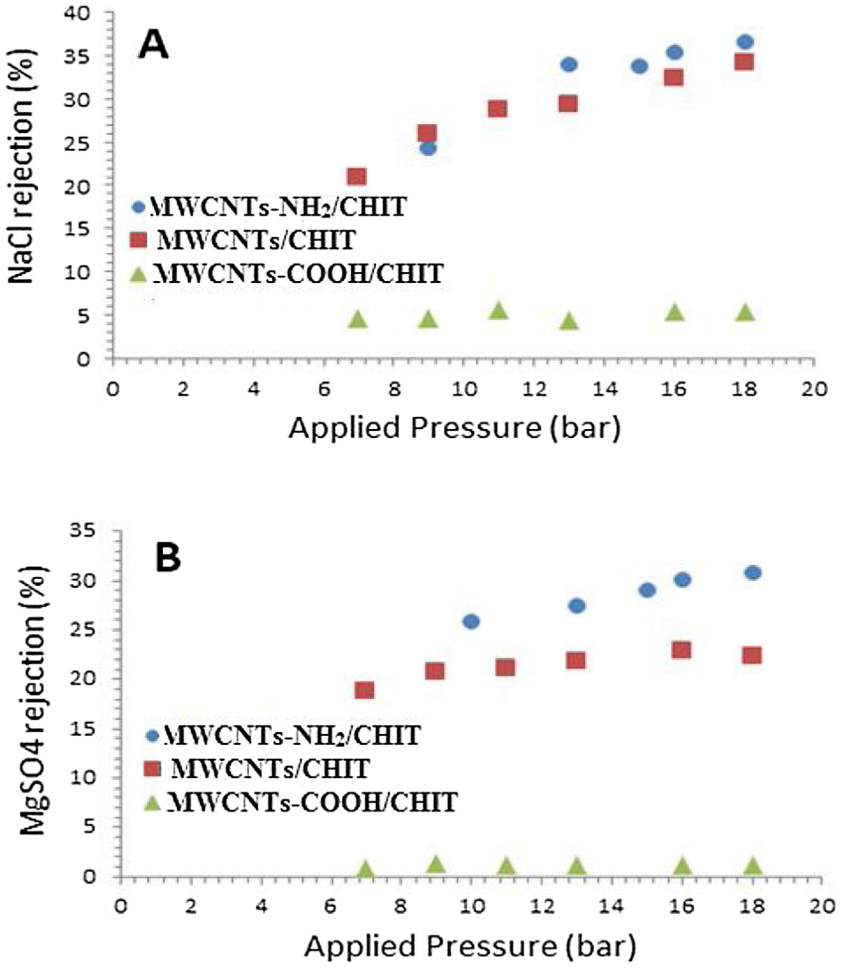

Fig. 9 – Comparison of the BP membranes' salt-rejection performances: A) observed rejection (%) of NaCl; B) observed rejection (%) of $MgSO_4$.

Table 3 – Comparison of pure and functionalized MWCNTs /chitosan membrane with other membranes in the literature for salt rejection.

Membrane materials	Membrane type	Rejection (%)		Ref.
		Base	Modified	
APTS-acid functionalized-CNT	NF	65.46	93.67	[70]
PCL-acid-functionalized-CNT	NF	8.65	26.71	[71]
TiO_2-acid functionalized-CNT	NF	69	80.7	[72]
PAA functionalized-CNT	NF	1.6	15.3	[73]
MWCNTs /chitosan	NF	6.1	66.3	This work

rejection of NaCl for two BP membranes (MWCNTs/chitosan, and MWCNTs-NH_2/chitosan) had increased by reduction the pH of the feed solution. This could be attributed to protonate of the amine groups ($NH_2+H^+ \leftrightarrow NH_3^+$), which are chiefly responsible for interactions with anions [68,69]. While the MWCNTs−COOH/chitosan membrane exhibited that, the NaCl rejection is lowest due to blockage of the free amino functional groups of chitosan during the crosslinking process [69]. A comparison of the salt rejection data collected from the litrature [70,71] utlizing various membranes containaing carbon nanotube with this work for nanofiltration is presented in Table 3. Summing up, the obtained data display that the fabricated membrane provides new exciting chances for nanofiltration membranes.

4. Conclusion

Three buckypaper membranes (MWCNTs/chitosan, MWCNTs−COOH/chitosan and MWCNTs-NH_2/chitosan) were fabricated applying a filtration method. The MWCNTs/chitosan BP membranes had the highest electrical conductivity, whereas the BP membranes (MWCNTs−COOH/chitosan and MWCNTs-NH_2/chitosan) had significantly lower electrical conductivity values.

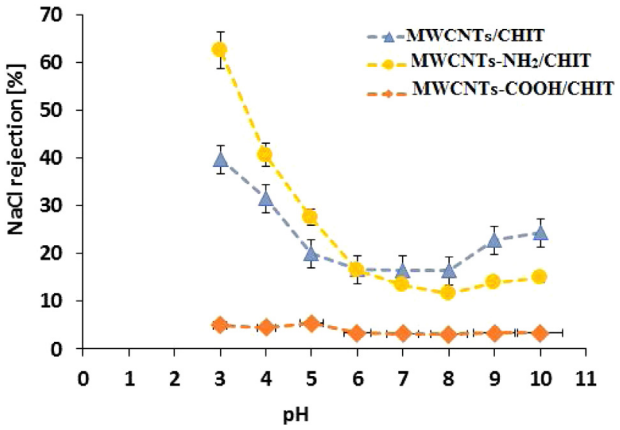

Fig. 10 – Comparison of salt-rejection performances of three BP membranes.

MWCNTs−COOH/chitosan BP membrane showed better mechanical properties than the other two BP membranes. On the other hand, COOH/chitosan BP membrane also had the highest permeate flux (6.6 ± 0.2 L/m2 h bar). This is attributed to the superior wettability and larger internal pores in the MWCNTs−COOH/chitosan BP, which plays a significant role in speeding the transportation of water molecules. While the results demonstrate that the single salt-rejection capacities (NaCl and $MgSO_4$) improved significantly when both MWCNTs/chitosan and MWCNTs-NH_2/chitosan BP membranes were used. This owing to presence of $–NH_2$ groups in the chitosan structure and the attachment to MWCNTs, which can be an effective adsorbent for salts from solution by its positive charge. In addition, crosslinking between the primary amine moieties of chitosan and the carboxylic groups on the walls of MWCNTs can result in low density of surface charges and larger internal pores. Therefore, the rejection capacity of single salts by MWCNTs−COOH/ chitosan BP was significantly decreased.

Conflict of interest

The authors declare no conflicts of interest.

Acknowledgment

This study was sponsored by King Abdul Aziz City for Science and Technology (KACST) and University of Wollongong. The authors appreciate the use of the facilities and the assistance of Dr. T. Romeo at the UOW Electron Microscopy Centre at University of Wollongong Australia.

REFERENCES

[1] Mekonnen MM, Gerbens-Leenes P, Hoekstra AY. Future electricity: the challenge of reducing both carbon and water footprint. Sci Total Environ 2016;569:1282–8.
[2] Song D, Xu J, Fu Y, Xu L, Shan B. Polysulfone/sulfonated polysulfone alloy membranes with an improved performance in processing mariculture wastewater. Chem Eng J 2016;304:882–9.
[3] Shannon PWBMark A, Elimelech Menachem, Georgiadis John G, Marin Benito J, Mayes Anne M. Science and technology for water purification in the coming decades. Nature 2008;452:301–10.
[4] Kayvani Fard A, McKay G, Buekenhoudt A, Al Sulaiti H, Motmans F, Khraisheh M, et al. Inorganic membranes: preparation and application for water treatment and desalination. Materials 2018;11:74.
[5] Zargar M, Hartanto Y, Jin B, Dai S. Polyethylenimine modified silica nanoparticles enhance interfacial interactions and desalination performance of thin film nanocomposite membranes. J Memb Sci 2017;541:19–28.
[6] Li Y, Yang S, Zhang K, Van der Bruggen B. Thin film nanocomposite reverse osmosis membrane modified by two dimensional laminar MoS2 with improved desalination performance and fouling-resistant characteristics. Desalination 2019;454:48–58.
[7] Werber JR, Osuji CO, Elimelech M. Materials for next-generation desalination and water purification membranes. Nat Rev Mater 2016;1:16018.
[8] Kakoria A, Sinha-Ray S. A review on biopolymer-based fibers via Electrospinning and solution blowing and their applications. Fibers 2018;6:45.
[9] Semiat R. Energy issues in desalination processes. Environ Sci Technol 2008;42:8193–201.
[10] Li D, Yan Y, Wang H. Recent advances in polymer and polymer composite membranes for reverse and forward osmosis processes. Prog Polym Sci 2016;61:104–55.
[11] Rangnekar N, Mittal N, Elyassi B, Caro J, Tsapatsis M. Zeolite membranes – a review and comparison with MOFs. Chem Soc Rev 2015;44:7128–54.
[12] Dong X-YQH, Zhang L, Cheng L-H, Chen H-L, Gao C-J. Preparation and characterization of surface-modified zeolite-polyamide thin film nanocomposite membranes for desalination. Desalin Water Treat 2011;34:6–12.
[13] Ahmed I, Khan NA, Jhung SH. Graphite Oxide/Metal–organic framework (MIL-101): remarkable performance in the adsorptive denitrogenation of model fuels. Inorg Chem 2013;52:14155–61.
[14] Chai PV, Mahmoudi E, Teow YH, Mohammad AW. Preparation of novel polysulfone-Fe3O4/GO mixed-matrix membrane for humic acid rejection. J Water Process Eng 2017;15:83–8.
[15] Pang R, Zhang K. Fabrication of hydrophobic fluorinated silica-polyamide thin film nanocomposite reverse osmosis membranes with dramatically improved salt rejection. J Colloid Interface Sci 2018;510:127–32.
[16] Abadikhah H, Kalali EN, Behzadi S, Khan SA, Xu X, Agathopoulos S. Amino functionalized silica nanoparticles incorporated thin film nanocomposite membrane with suppressed aggregation and high desalination performance. Polymer 2018;154:200–9.
[17] Zhao F-Y, Ji Y-L, Weng X-D, Mi Y-F, Ye C-C, An Q-F, et al. High-flux positively charged nanocomposite nanofiltration membranes filled with poly(dopamine) modified multiwall carbon nanotubes. ACS Appl Mater Interfaces 2016;8:6693–700.
[18] Zhao H, Qiu S, Wu L, Zhang L, Chen H, Gao C. Improving the performance of polyamide reverse osmosis membrane by incorporation of modified multi-walled carbon nanotubes. J Memb Sci 2014;450:249–56.
[19] Vatanpour V, Madaeni SS, Moradian R, Zinadini S, Astinchap B. Novel antibifouling nanofiltration polyethersulfone membrane fabricated from embedding TiO2 coated multiwalled carbon nanotubes. Sep Purif Technol 2012;90:69–82.

[20] Kim E-S, Hwang G, Gamal El-Din M, Liu Y. Development of nanosilver and multi-walled carbon nanotubes thin-film nanocomposite membrane for enhanced water treatment. J Memb Sci 2012;394-395:37–48.
[21] Alshahrani AA, Al-Zoubi H, Nghiem LD, Panhuis Minhet. Synthesis and characterisation of MWNT/chitosan and MWNT/chitosan-crosslinked buckypaper membranes for desalination. Desalination 2017;418:60–70.
[22] Zhou S, Hrymak AN, Kamal MR. Electrical, morphological and thermal properties of microinjection molded polyamide 6/multi-walled carbon nanotubes nanocomposites. Compos Part A Appl Sci Manuf 2017;103:84–95.
[23] Chiu F-C, Chuang Y-C, Liao S-J, Chang Y-H. Comparison of PVDF/PVAc/GNP and PVDF/PVAc/CNT ternary nanocomposites: enhanced thermal/electrical properties and rigidity. Polym Test 2018;65:197–205.
[24] Sohrabi S, Dehghanpour S, Ghalkhani M. A cobalt porphyrin-based metal organic framework/multi-walled carbon nanotube composite electrocatalyst for oxygen reduction and evolution reactions. J Mater Sci 2018;53:3624–39.
[25] Wu H, Tang B, Wu P. Novel ultrafiltration membranes prepared from a multi-walled carbon nanotubes/polymer composite. J Memb Sci 2010;362:374–83.
[26] Sweetman LJ. Synthesis, characterisation and applications of carbon nanotube membranes containing macrocycles and antibiotics; 2012.
[27] Ihsanullah. Carbon nanotube membranes for water purification: developments, challenges, and prospects for the future. Sep Purif Technol 2019;209:307–37.
[28] Wang N, Tang Z-K, Li G-D, Chen J. Materials science: single-walled 4 Å carbon nanotube arrays. Nature 2000;408:50.
[29] Qin L-C, Zhao X, Hirahara K, Miyamoto Y, Ando Y, Iijima S. Materials science: the smallest carbon nanotube. Nature 2000;408:50.
[30] Dumée LF, Sears K, Schütz J, Finn N, Huynh C, Hawkins S, et al. Characterization and evaluation of carbon nanotube Bucky-Paper membranes for direct contact membrane distillation. J Memb Sci 2010;351:36–43.
[31] Ribeiro B, Botelho EC, Costa ML, Bandeira CF. Carbon nanotube buckypaper reinforced polymer composites: a review. Polímeros 2017;27:247–55.
[32] Sohrabi B, Poorgholami-Bejarpasi N, Nayeri N. Dispersion of carbon nanotubes using mixed surfactants: experimental and molecular dynamics simulation studies. J Phys Chem B 2014;118:3094–103.
[33] Geng Y, Liu MY, Li J, Shi XM, Kim JK. Effects of surfactant treatment on mechanical and electrical properties of CNT/epoxy nanocomposites. Compos Part A Appl Sci Manuf 2008;39:1876–83.
[34] Hill DE, Lin Y, Rao AM, Allard LF, Sun Y-P. Functionalization of carbon nanotubes with polystyrene. Macromolecules 2002;35:9466–71.
[35] Diez-Pascual A, Naffakh M, Gómez M, Marco C, Ellis G, Gonzalez-Dominguez J, et al. The influence of a compatibilizer on the thermal and dynamic mechanical properties of PEEK/carbon nanotube composites. Nanotechnology 2009;20:315707.
[36] Spitalsky Z, Tasis D, Papagelis K, Galiotis C. Carbon nanotube–polymer composites: chemistry, processing, mechanical and electrical properties. Prog Polym Sci 2010;35:357–401.
[37] Bilalis P, Katsigiannopoulos D, Avgeropoulos A, Sakellariou G. Non-covalent functionalization of carbon nanotubes with polymers. RSC Adv 2014;4:2911–34.
[38] Morishita T, Matsushita M, Katagiri Y, Fukumori K. Noncovalent functionalization of carbon nanotubes with maleimide polymers applicable to high-melting polymer-based composites. Carbon 2010;48:2308–16.
[39] Horváth G, Kawazoe K. Method for the calculation of effective pore size distribution in molecular sieve carbon. J Chem Eng Jpn 1983;16:470–5.
[40] Barrett EP, Joyner LG, Halenda PP. The determination of pore volume and area distributions in porous substances. I. Computations from nitrogen isotherms. J Am Chem Soc 1951;73:373–80.
[41] Zhang Y, Zhang X, Ding R, Zhang J, Liu J. Determination of the degree of deacetylation of chitosan by potentiometric titration preceded by enzymatic pretreatment. Carbohydr Polym 2011;83:813–7.
[42] Kalut SA. Enhancement of degree of deacetylation of chitin in chitosan production. UMP 2008.
[43] Qinna NA, Karwi QG, Al-Jbour N, Al-Remawi MA, Alhussainy TM, Al-So'ud KA, et al. Influence of molecular weight and degree of deacetylation of low molecular weight chitosan on the bioactivity of oral insulin preparations. Mar Drugs 2015;13:1710–25.
[44] Tabriz A, Alvi MAUR, Niazi MBK, Batool M, Bhatti MF, Khan AL, et al. Quaternized trimethyl functionalized chitosan based antifungal membranes for drinking water treatment. Carbohydr Polym 2019;207:17–25.
[45] Shakeri A, Salehi H, Rastgar M. Chitosan-based thin active layer membrane for forward osmosis desalination. Carbohydr Polym 2017;174:658–68.
[46] Branca C, D'Angelo G, Crupi C, Khouzami K, Rifici S, Ruello G, et al. Role of the OH and NH vibrational groups in polysaccharide-nanocomposite interactions: a FTIR-ATR study on chitosan and chitosan/clay films. Polymer 2016;99:614–22.
[47] Sweetman LJ, Moulton SE, Wallace GG. Characterisation of porous freeze dried conducting carbon nanotube–chitosan scaffolds. J Mater Chem 2008;18:5417–22.
[48] Moulton SE, Minett AI, Murphy R, Ryan KP, McCarthy D, Coleman JN, et al. Biomolecules as selective dispersants for carbon nanotubes. Carbon 2005;43:1879–84.
[49] Brunauer S, Emmett PH, Teller E. Adsorption of gases in multimolecular layers. J Am Chem Soc 1938;60:309–19.
[50] Boge J, Sweetman LJ, Ralph SF. The effect of preparation conditions and biopolymer dispersants on the properties of SWNT buckypapers. J Mater Chem 2009;19:9131–40.
[51] Jenny Boge, Sweetman LJ, in het Panhuis M, Ralph SF. The effect of preparation conditions and biopolymer dispersants on the properties of SWNT buckypapers. J Mater Chem 2009;19:9131–40.
[52] Sweetman LJ. Synthesis, characterisation and applications of carbon nanotube membranes containing macrocycles and antibiotics. Dissertation/Thesis, School of Chemistry, Wollongong University; 2012.
[53] Sing KS. Physisorption of nitrogen by porous materials. J Porous Mater 1995;2:5–8.
[54] Sweetman L, Nghiem L, Chironi I, Triani G, Ralph SF. Synthesis, properties and water permeability of SWNT buckypapers. J Mater Chem 2012;22:13800–10.
[55] Whitten PG, Gestos AA, Spinks GM, Gilmore KJ, Wallace GG. Free standing carbon nanotube composite bio-electrodes. J Biomed Mater Res Part B Appl Biomater 2007;82: 37–43.
[56] Frizzell C, Coutinho D, Balkus K Jr, Minett AI, Blau W, Coleman J. Reinforcement of macroscopic carbon nanotube structures by polymer intercalation: the role of polymer molecular weight and chain conformation. Phys Rev B 2005;72:245420.
[57] Salam MA, Makki MS, Abdelaal MY. Preparation and characterization of multi-walled carbon nanotubes/chitosan nanocomposite and its application for the removal of heavy

metals from aqueous solution. J Alloys Compd 2011;509:2582–7.
[58] Childress AE, Elimelech M. Relating nanofiltration membrane performance to membrane charge (electrokinetic) characteristics. Environ Sci Technol 2000;34:3710–6.
[59] Childress AE, Elimelech M. Effect of solution chemistry on the surface charge of polymeric reverse osmosis and nanofiltration membranes. J Memb Sci 1996;119:253–68.
[60] Tu KL, Chivas AR, Nghiem LD. Effects of membrane fouling and scaling on boron rejection by nanofiltration and reverse osmosis membranes. Desalination 2011;279:269–77.
[61] Schäfer A, Pihlajamäki A, Fane AG, Waite T, Nyström M. Natural organic matter removal by nanofiltration: effects of solution chemistry on retention of low molar mass acids versus bulk organic matter. J Memb Sci 2004;242:73–85.
[62] Xu G, Nie P, Dou H, Ding B, Li L, Zhang X. Exploring metal organic frameworks for energy storage in batteries and supercapacitors. Mater Today 2017;20:191–209.
[63] Huang R, Chen G, Sun M, Hu Y, Gao C. Studies on nanofiltration membrane formed by diisocyanate cross-linking of quaternized chitosan on poly (acrylonitrile)(PAN) support. J Memb Sci 2006;286:237–44.
[64] Lee S, Shim Y, Kim IS, Sohn J, Yim S, Cho J. Determination of mass transport characteristics for natural organic matter (NOM) in ultrafiltration (UF) and nanofiltration (NF) membranes. Water Sci Technol Water Supply 2002;2:151–60.
[65] Wu P, Wu H, Tang B. Novel ultrafiltration membranes prepared from a multi-walled carbon nanotubes/polymer composite. J Memb Sci 2010;362:374–83.
[66] Hussain MR, Iman M, Maji TK. Determination of degree of deacetylation of chitosan and their effect on the release behavior of essential oil from chitosan and chitosan-gelatin complex microcapsules. International Journal of Advanced Engineering Applications 2013;6:4–12.
[67] Millero FJ. Molal volumes of electrolytes. Chem Rev 1971;71:147–76.
[68] Saifuddin M, Kumaran P. Removal of heavy metal from industrial wastewater using chitosan coated oil palm shell charcoal. Electron J Biotechnol 2005;8:43–53.
[69] Amuda O, Giwa A, Bello I. Removal of heavy metal from industrial wastewater using modified activated coconut shell carbon. Biochem Eng J 2007;36:174–81.
[70] Zeng G, He Y, Yu Z, Yang X, Yang R, Zhang L. J Chem Technol Biotechnol 2016;91:2322–30.
[71] Mansourpanah Y, Madaeni SS, Rahimpour A, Adeli M, Hashemi MY, Moradian MR. Desalination 2011;277:171–7.
[72] Vatanpour V, Madaeni SS, Moradian R, Zinadini S, Astinchap B. Sep Purif Technol 2012;90:69–82.
[73] Daraei P, Madaeni SS, Ghaemi N, Khadivi MA, Astinchap B, Moradian R. J. Membr. Sci 2013;444:184–91.